TRENDS IN SCIENCES 2025; 22(11): 10305
https://doi.org/10.48048/tis.2025.10305 RESEARCH ARTICLE

Design and Study of Nano-Composite Materials based Transparent Conductive Electrode using Green Synthesis method for Solar Cells

Yaddanapudi Venkata Bhaskara Lakshmi[1], K. Saujanya[2,*], Satheesh Ampolu[3], Jayarangarao Prathipati[1], Suneel Kumar Asileti[4], Hanumanthu Usha[5], Ravi Kota[6] and Narasimhulu Tamminana[1]

[1]*Baba Institute of Technology and Sciences, Visakhapatnam, Andhra Pradesh,530048, India*
[2]*Vignan's Institute of Information Technology, Visakhapatnam, Andhra Pradesh, 530003, India*
[3]*Department of Chemistry, Centurion University of Technology and Management, Vizianagaram 535002, India*
[4]*Usha Rama College of Engineering and Technology, Telaprolu, Andhra Pradesh, 521109, India*
[5]*Department of Chemistry, Government Polytechnic for Women, Srikakulam, Andhra Pradesh,532005, India*
[6]*Sanketika Vidya Parishad Engineering College-AU, Visakhapatnam, Andhra Pradesh, 521109, India*

([*]Corresponding author's e-mail: saujanya433@gmail.com)

Received: 5 April 2025, Revised: 13 June 2025, Accepted: 20 June 2025, Published: 5 August 2025

Abstract

The fabrication of transparent electrodes using green-synthesized nanoparticles offers an eco-friendly, cost-effective, and efficient alternative to conventional clean-room methods. The spin coating technique was used to fabricate a transparent electrode utilizing green synthesized ZTO (Zinc Tin Oxide) Nano composites and MgF_2 (Magnesium Fluoride) nanoparticles. In this procedure, glass substrate rotating at 4000 rpm is spin-coated with green synthesized ZTO nanoparticles at varying rotational speeds. For 5000, 6000, and 8000 rpms, follow the same steps. The samples were then dried for an h at 60 °C in a hot air oven. Subsequently, ZTO samples operating at 2000 rpm are covered with MgF_2. For the remaining samples, use the same process. There was no discernible conductivity even with a high level of transparency. Finally, on top of MgF_2, the conducting polymer PEDOT:PSS is placed. This step completed the fabrication of the transparent electrode. Advanced electronic and optoelectronic devices can benefit from the excellent electrical conductivity and transparency of tin-doped zinc oxide (ZTO) films and multilayer combined with other conducting materials. To examine optical and electrical characteristics, UV-visible spectroscopy and a frequency/impedance analyser were utilised. The study determined that the best combination for performance analysis using the GPVDM (General-purpose Photovoltaic Device Model) simulator was 1:1 ZTO nanoparticles extracted with Aloe barbadensis mill and anti-reflection coating as MgF^2 as a second layer and PEDOT:PSS as a tri layer. The modeling findings showed that a number of common transparent electrodes used in solar cells may be effectively replaced by green ZTO nanoparticles coated in many layers.

Keywords: Tin Doped Zinc Oxide (ZTO), Solar cell, Transmission, GPVDM simulation, Transparent electrodes, Aloe barbadensis mill

Introduction

Because of their superior electrical and optical qualities, transparent conducting oxide thin films have found extensive use in recent years in a variety of electronic applications. These include organic and dye-sensitized solar cells[1-4], laser diodes Nair *et al.* [5], Cao *et al.* [6], photodiodes [7-11], light-emitting diodes Han *et al.* [12], El-Shaer *et al.* [13], piezoelectric devices Saxena *et al.* [14], Ueda *et al.* [15], acoustic waveguides [16], and many more. These transparent conducting

films have a significant optical band gap energy, low resistance, and very high optical transmittance. In optoelectronic devices, transparent thin films composed of indium tin oxide (ITO) are most frequently used. ZTO thin films are very compatible with many processes and may be produced by both solution-based and vacuum-based methods [17,18]. ZTO Thin films are capable of created synthetically using many methods, including chemical vapour deposition, atomic layer deposition, RF/DC sputtering, sol-gel spin coating, and others [19-22]. When compared to other metal oxide materials, which are primarily byproducts of refining processes, the resources needed for ZTO are abundant on Earth; however, these metal oxides have limited resources, and in the near future, some of them like gallium and indium may completely deplete. Comparably, materials with combined optical, electrical, and thermal characteristics—such as conducting polymers—have shown to be advantageous for technology. Conducting polymers are used in a wide range of highly specialised industrial applications, such as LEDs, sensors, electrodes, solar cells, super capacitor materials, and many more [23]. The scientific community has shown interest in the conducting polymer family polythiophene and its derivatives, such as poly(3-methylthiophene), poly(3-hexylthiophene), and poly(3,4-ethylenedioxythiophene) (PEDOT), due to its potential technological uses. Polystyrenesulfonate (PSS), which has exceptional stability, flexible mechanical qualities, and very high transparency, can be added to PEDOT to improve its water solubility. In the realm of transparent conductors, the PEDOT:PSS polymer system presents a competitive alternative to established technologies[24]. These days, photovoltaic applications are using it a lot [25].

Promising in terms of UV transparency, MgF2 thin film is comparable to other large band gap fluorides and oxides, such as LaF3 and Al2O3, respectively [26,27]. The rutile crystal structure of bulk magnesium fluorite has a large band gap of about 12.8 eV and a low refractive index of 1.38 [28,29]. The top of the cell is coated with a single layer of magnesium fluoride (MgF2) to act as an anti-reflective material and promote photon absorption from input light. This process increases the generation of electron-hole pairs in the absorber layer [30]. Multilayers based on MgF2 thin films have been applied to several optical applications, such as UV laser high-reflective coatings [31]. Electromagnetic shielding and flat panel displays are 2 applications for MgF2 thin film multilayers made of conducting materials and indium tin. The fabrication of ZTO multilayer thin films utilizing the spin coating process is the main focus of the current research effort. The link between optical transparency and wavelength and AC conductivity and frequency was defined by tests of optical and electrical conductivity conducted at room temperature and at different wavelengths and frequencies [32].

Materials and methods

Zinc and tin chloride were added to the precursor solution at a ratio of one to one. The aforesaid solution was combined with the mineralizing leaf extracts from Terminaliacatappa and Aloe barbadensis mill in 2 different containers. Test bacteria and fungi were cultured on Mueller-Hinton and Sabouraud's Dextrose Agar plates, respectively, using sterile cotton swabs. Five 6 mm wells were made in each plate, and 50 µL of each compound and positive control (Streptomycin, 100 µg/mL) was added. Plates were left at room temperature for 1 h, then incubated at 37 °C for 24 h. Inhibition zones were measured to assess antimicrobial activity. Zinc stannate nanoparticles (ZTO NPs) were synthesized using plant extracts (Aloe barbadensis mill and Terminalia catappa) or NaOH. Media preparation involved autoclaving and pH adjustment, followed by sterile plate pouring for microbial testing. To achieve a flawless blending of the leaf extracts and chemical precursors, these containers were subjected to magnetic churning for approximately 3 h. After that, the thick solution was gradually poured into a Teflon container that was fitted with a stainless-steel autoclave. For a full day, the autoclave is kept at or close to 200 ℃. After that, the powders were cleaned and burned for 4 h at 600 ℃. Consequently, the resulting materials were given the designations after being processed into fine powders, ZTO 11A (leaf extract: Aloe barbadensis mill) and 11B (leaf extract: Terminaliacatappa) [33,34]. The process of chemosynthesis of ZTO nanoparticles was carried out in a similar manner, using NaOH solution as the mineralizer and capable of maintaining the reaction media's pH at a steady level. ZTO was the name of the powder that was eventually created.

Synthesis of magnesium fluoride (MgF2) nanoparticles

Terminaliacatappa (Indian Badam) leaf extract was used as a reducing agent in the production of MgF_2 nanoparticles. The stoichiometric ratio of $MgCl_2$ and ammonium fluoride (NH_4F_2) was mixed in a beaker using a magnetic stirrer, and then the Terminaliacatappa leaf extract was added dropwise. After 3 h of stirring, the final solution was centrifuged for 24 h at 6000 rpm. Centrifugation produced a white, crystalline powder, which was then repeatedly washed and dried in a hot air oven.

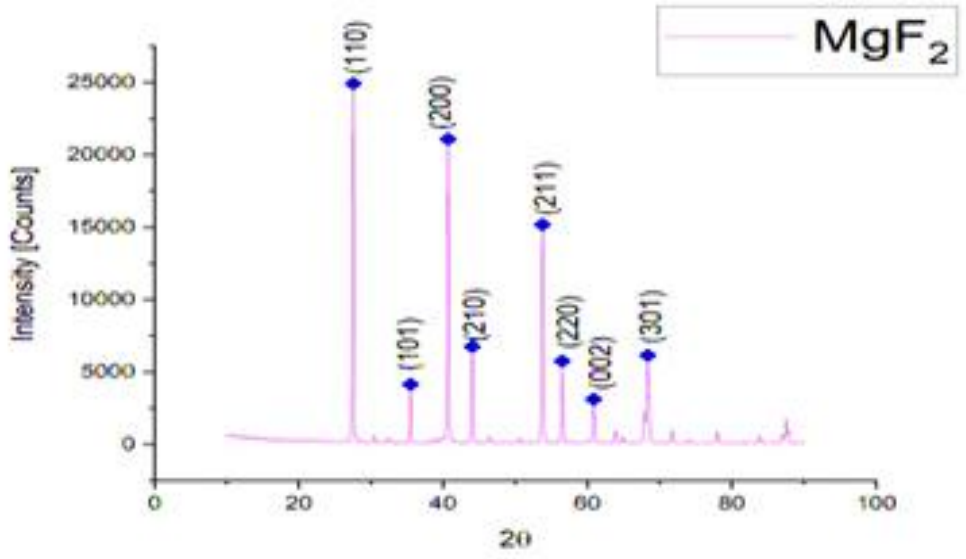

Figure 1 X-Ray Diffraction pattern of Magnesium Fluoride (MgF_2) nanoparticles.

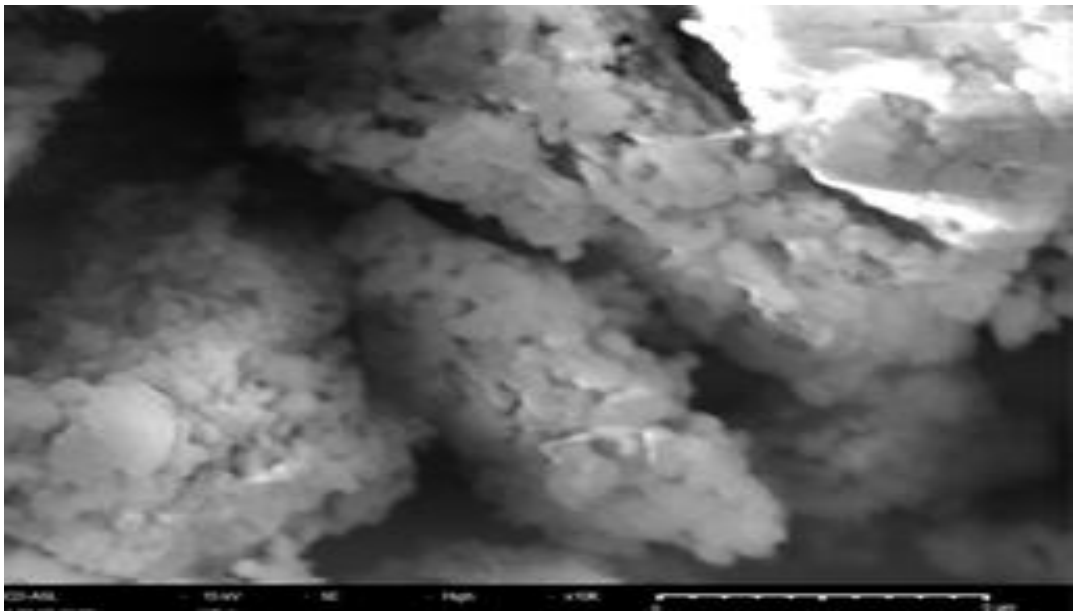

Figure 2 Scanning Electron Microscopy of Magnesium Fluoride (MgF_2) nanoparticles.

Characterization

Using a nickel filter CuKα radiation, the resulting magnesium fluoride (MgF_2) nanoparticles are characterized at room temperature. ($\lambda = 1.54059$ Å) over a wide range of $10^o \leq 2\theta \leq 80^o$ at a scanning speed of 2 min^{-1} using an X-ray diffractometer (PAN analytical-X' Pert PRO, Japan)as shown in **Figure 1**. The measurement carried out with voltage 40KV and current

40mA was to determine the crystallinity of nano-particles. About 5.0gms of the dried ZnSnO3 NPs were deposited as a randomly oriented powder on to a plexiglass sample container. The diffraction planes 2θ (104), (110), (105) and (006) were obtained at 32.1º, 34.4º, 36.5º and 38.6º, respectively, corresponding to the standard $ZnSnO_3$ material with JCPDS File No. 11-0274 [35,36]. UV-vis spectra were recorded using a single monochromator UV-2600 (optionally an ISR-2600Plus, λ up to 1400 nm). Scanning electron microscopy was used to analyze the morphology of the materials as they were synthesized (SEM, LEO1550) Soin *et al.* [33], Bhaskaralakshmi *et al.* [37] shown in **Figure 2**.

Conducting polymer

The well-known conducting polymer polystyrene sulfonate (PEDOT:PSS) was acquired from Sigma Aldrich in the USA as an aqueous dispersion of high conductivity grade 3.0% TO 4.0% in H_2O [12,38].

Preparation of thin films

Zinc tin oxide (ZTO) nanoparticles were diluted by 1:1 molar ratio with the ethanol as a solvent. ZTO film was coated on glass substrates using spin coater at 4000, 5000, 6000, and 8000 RPM. The coated glass substrates were removed and dried at 80 °C for an h in a hot air oven. The prepared thin films were assigned names as 11A4K, 11A5K, 11A6K, and 11A8Krespectively. The Transmittance and the conductivity were measured using UV VIS spectroscopy and impedance analyzer.

Preparation of thin film sample 2

The above mentioned ZTO thin films were coated again with magnesium fluoride (MgF2) to achieve high optical transparency which is one of the prerequisites of transparent electrodes. The coated (ZTO+MgF2) thin films were again assigned names as 11A4KM, 11A5KM, 11A6KM, and 11A8KM respectively. In order to measure the transmittance and conductivity, impedance analysis and UV-VIS spectroscopy were used.

Preparation of thin film sample 3

Polyethylene dioxythiophene: polystyrene sulfonate (PEDOT:PSS) which is a well-known conducting polymer, as an aqueous dispersion of high conductivity grade was purchased from Merck India and was coated over ZTO thin films to prepare ZTO+PEDOT:PSS thin films. According to recent studies, PEDOT:PSS formulations can be employed as transparent contacts in solar cell applications, providing superior [39].

In addition, spin coating was performed on a spin coater for 30 s and later on dried at 80 °C for an h in a hot air oven. The prepared thin films were assigned names as 11A4KP, 11A5KP, 11A6KP, and 11A8KP respectively. The Transmittance and the conductivity were measured using UV-Vis spectroscopy and impedance analyzer.

Preparation of thin film sample 4

ZTO+MgF_2 thin film samples were coated with PEDOT:PSS once more using the previously described protocol to produce ZTO+MgF_2+PEDOT:PSS thin films. The designations 11A4KMP, 11A5KMP, 11A6KMP, and 11A8KMP were given to the prepared thin films, in that order. An impedance analyzer and UV-VIS spectroscopy were used to measure the conductivity and transmittance [39,40]. This is the final coated film.

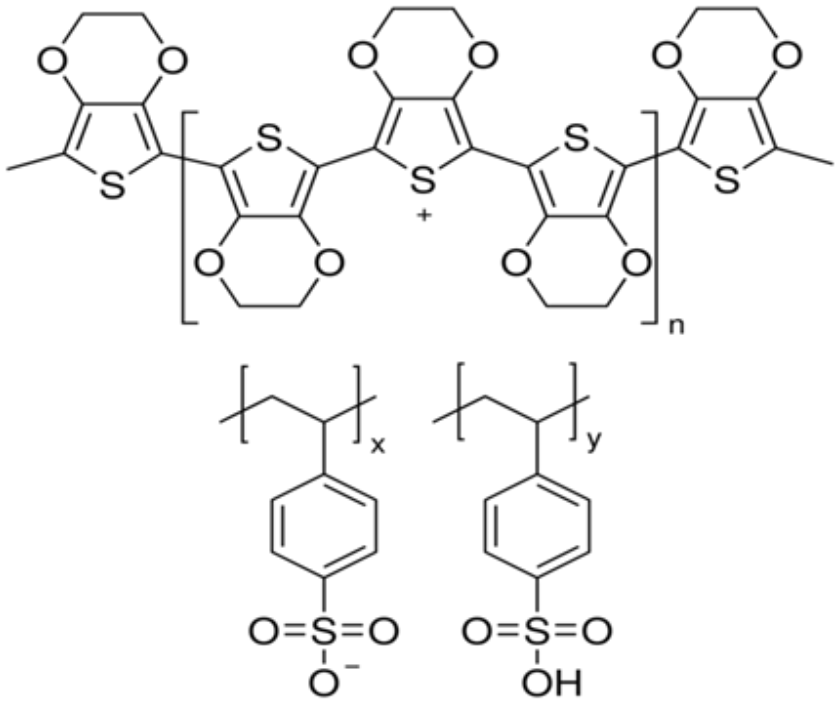

Figure 3 Polyethylene dioxythiophene: Polystyrene sulfonate (PEDOT:PSS) results.

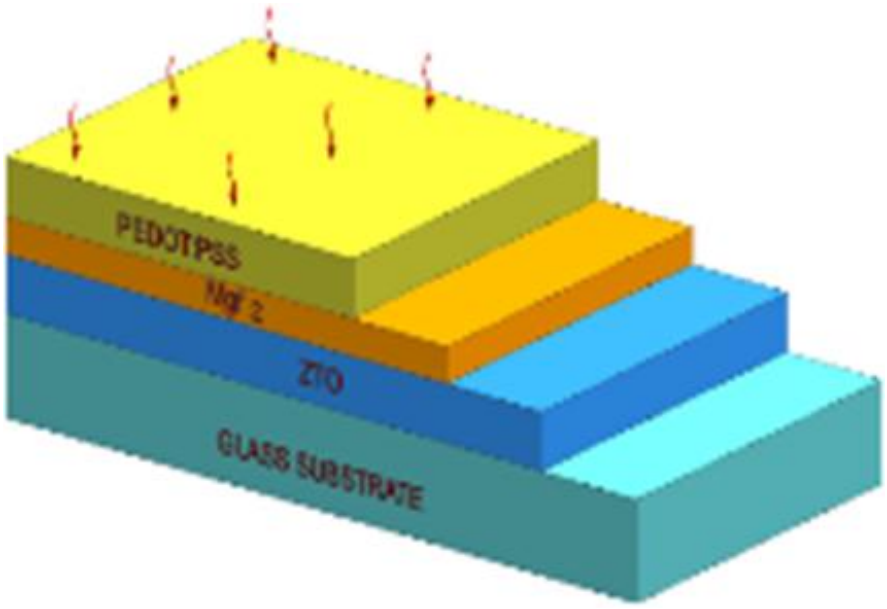

Figure 4 Architecture of transparent electrode.

Results and discussion

Optical Studies

Wavelength VS Transmission % (A) Transmission % of 11A4K, 11A5K, 11A6K, and 11A8k thin films at various wavelengths is shown in **Figure 5**. (B) Transmission percentage at various wavelengths of thin films 11A4KM, 11A5KM, 11A6KM, and 11A8KM (C)Transmission percentage of thin films with 11A4KP, 11A5KP, 11A6KP, and 11A8KP at various wavelengths (D) Transmission percentage at various wavelengths of thin films with 11A4KMP, 11A5KMP, 11A6KMP, and 11A8KMP. Observing **Figures 5(A) - 5(D)**, where transparency rises with decreasing thickness or greater rotation speed. The greatest feasible transparency in **Figure 5(A)** is 90, while in **Figure 5(B)** it ranges from 92% to 93%. The highest attainable transparency below

90% is shown in **Figure 5(C)**. **Figure 5(D)** shows the films coated with PEDOT, ZTO, and MgF_2: In the UV, VIS, and IR areas, the maximum perceptible transparency is between 92% and 98%. PSS displays appreciable transparency percentage at all RPMs.

Electrical characteristics

Electrical conductivity of ZTO-based thin films was measured using a PSM 1735 Frequency Response Analyzer across 1 kHz to 10 MHz at room temperature. Four different sample configurations were analyzed:

- **Sample-1 (ZTO on glass):** Maximum conductivity ~1.6×10^{-8} S/cm at most spinning speeds; significant drop (0.75×10^{-9} S/cm) at 8000 RPM due to reduced film thickness.
- **Sample-2 (ZTO + MgF_2 on glass):** Consistent conductivity around ~1.5×10^{-8} S/cm across all speeds; spinning speed had minimal effect.
- **Sample-3 (ZTO + PEDOT:PSS on glass):** Highest conductivity ~4×10^{-8} S/cm at 4000 RPM; reduced at higher speeds due to thinner films.
- **Sample-4 (ZTO + MgF_2 + PEDOT:PSS on glass):** Conductivity peaked at ~3×10^{-8} S/cm at 4000 RPM; dropped significantly at higher speeds.

Sample-4 exhibited the best combined electrical and optical performance and was chosen for further statistical modeling using GPVDM, with potential application as a transparent electrode in solar cells.

The conductivity of thin films 11A4K, 11A5K, 11A6K, and 11A8k at various frequencies is plotted against frequency in **Figure 6**. (B) The conductivity of thin films 11A4K, 11A5K, 11A6K, and 11A8k at various frequencies is plotted against frequency in **Figure 6**. (B) The conductivity of thin films with 11A4KM, 11A5KM, 11A6KM, and 11A8KM at various frequencies. (C) The conductivity of thin films with 11A4KP, 11A5KP, 11A6KP, and 11A8KP at various frequencies. (D) Conductivity of thin films with 11A4KMP, 11A51KMP, 11A6KMP, and 11A8KMP at various frequencies. A graph showing the relationship between the frequency and conductivity of the films prepared at various RPMs is created based on electrical properties on Impedance analyzer. The results shows that the prepared film is conducting for a wide range of frequencies. The conductivity is observed to be in the order of 10^{-8}A in **Figures 6(A) - 6(B)**. **Figures 6(C) - 6(D)** show that the conductivity increases with frequency and is also in the order of 10^{-8}A. **Figure 6(D)** illustrates a notable conductivity on the order of 10^{-8}A with a high value among the films sold.

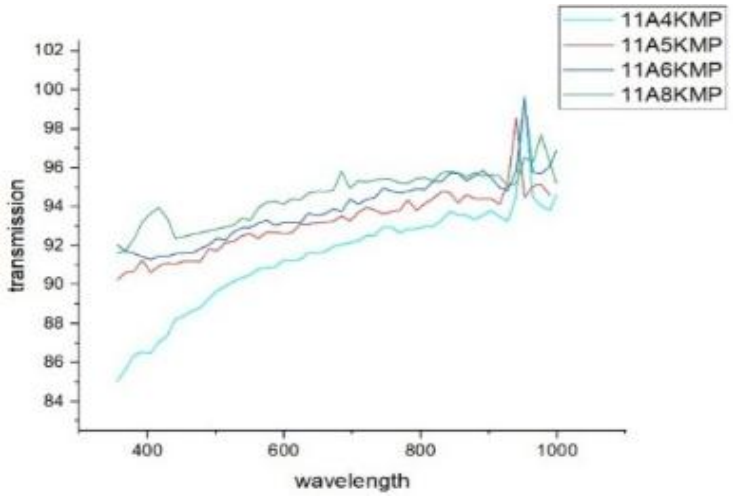

(A)

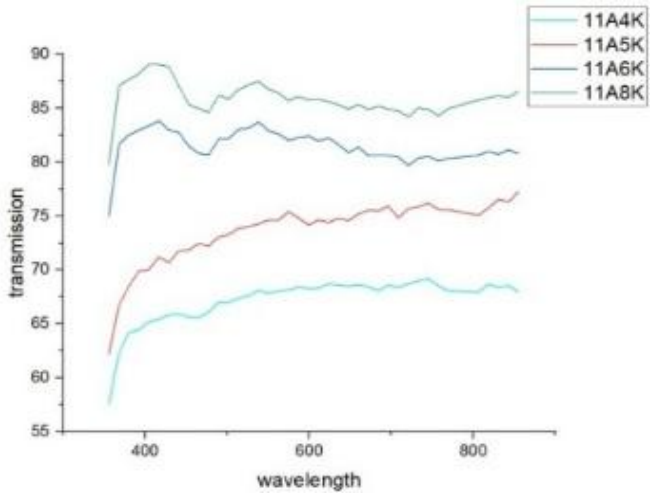

(B)

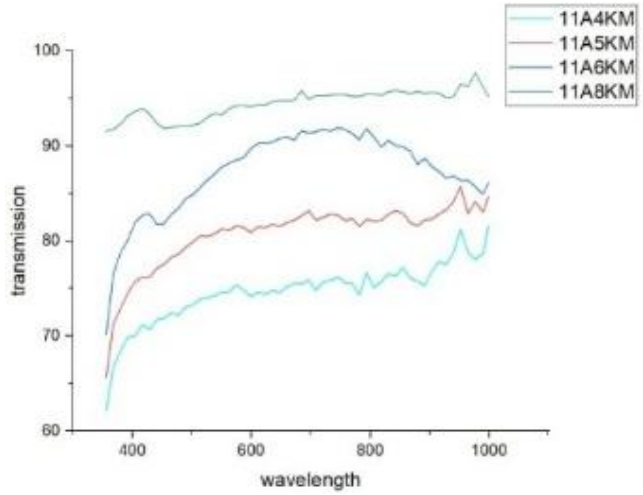

(C)

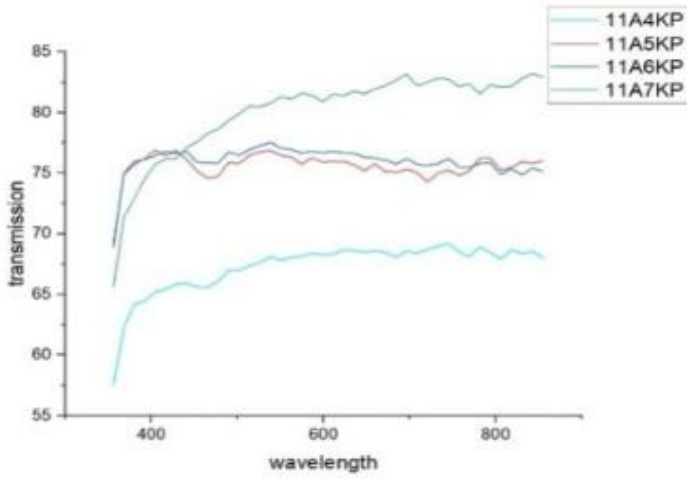

(D)

Figure 5 Wavelength VS Transmission % (A) Transmission % of 11A4K, 11A5K, 11A6K, and 11A8k thin films at different wavelengths. (B) Transmission % of 11A4KM, 11A5KM, 11A6KM, and 11A8KM thin films at different wavelengths d (C)Transmission % of 11A4KP, 11A5KP, 11A6KP, and 11A8KP thin films at different wavelengths (D) Transmission % of 11A4KMP, 11A5KMP, 11A6KMP, and 11A8KMP thin films at different wavelengths.

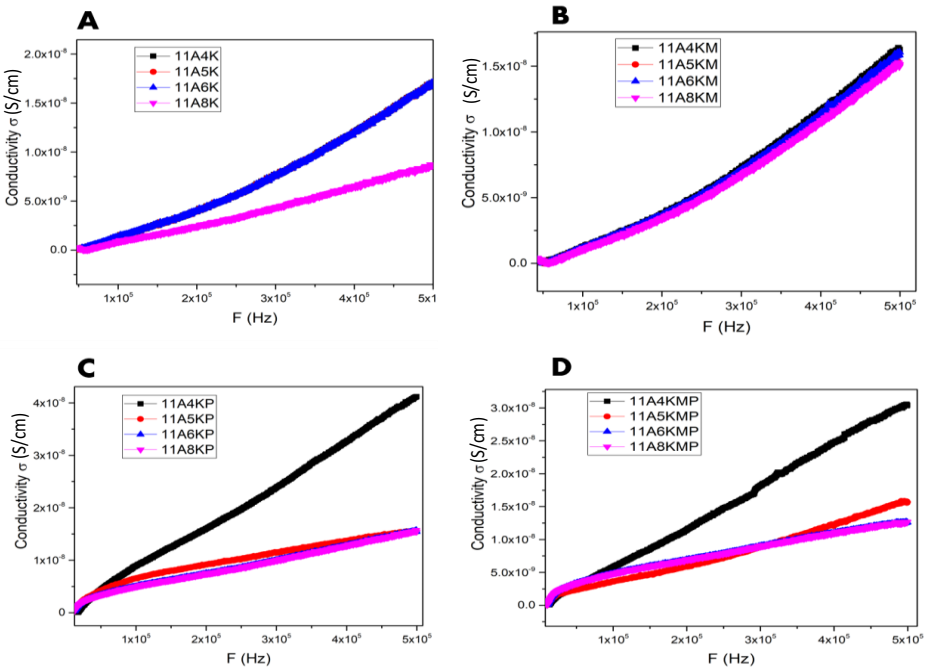

Figure 6 Conductivity vs Frequency (A) Conductivity of 11A4K, 11A5K, 11A6K, and 11A8K thin films at different frequencies. (B) Conductivity of 11A4KM, 11A5KM, 11A6KM, and 11A8KM thin films at different frequencies. (C) Conductivity of 11A4KP, 11A5KP, 11A6KP, and 11A8KP thin films at different frequencies. (D) Conductivity of 11A4KMP, 11A51KMP, 11A6KMP, and 11A8KMP thin films at different frequencies.

Statistical analysis using GPVDM simulation

The General-Purpose Photovoltaic Device Model (GPVDM) is an open-source simulation software designed for modeling optoelectronic devices such as solar cells, LEDs, and photodetectors. It solves the coupled differential equations governing charge carrier transport, optical absorption, and recombination dynamics in multilayer devices using a drift-diffusion framework.

In this study, GPVDM was used to simulate the electrical and optical performance of the thin film solar cells comprising green-synthesized ZTO, MgF_2, and PEDOT:PSS layers. Key input parameters included the thickness, refractive index (n), extinction coefficient (k), dielectric constant, electron/hole mobility, and defect densities. The software enabled analysis of device characteristics such as current–voltage (J–V) behavior, electric field distribution, generation and recombination rates, and efficiency performance under standard AM1.5G illumination.The GPVDM platform is particularly useful for predicting the influence of material properties and layer architectures on device performance, providing a valuable comparison to experimental results.

a. Optical Characterization: The optical model provides the experimental refractive index (n), absorption coefficient (α) (m−1) of the film as a function of λ (nm), and the absorbed photons at each place in the device.

"According to **Figure 7**, the distribution of photon density declines for samples created at varied spinning speeds from the surface (y = 0) to the top of the active layer. In the visible area, thinner films exhibit higher photon densities and absorbed photon densities when compared to thicker films. The absorbed photon density is observed to rise with thickness (nm), as illustrated in **Figures 7(a) - 7(d)**, and **Figures 8(a) - 8(d)**, and **Table 1**.

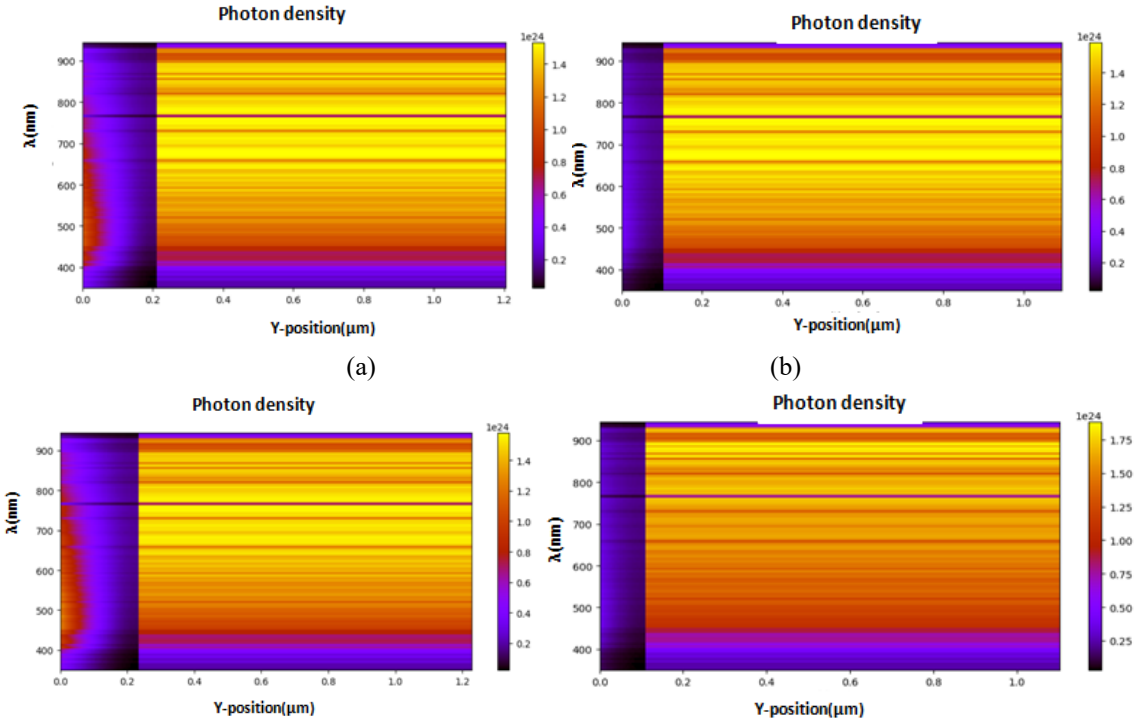

Figure 7 Photon density plots for samples developed at (a) 4000 (b) 5000 (c) 6000, and (d) 8000 RPM.

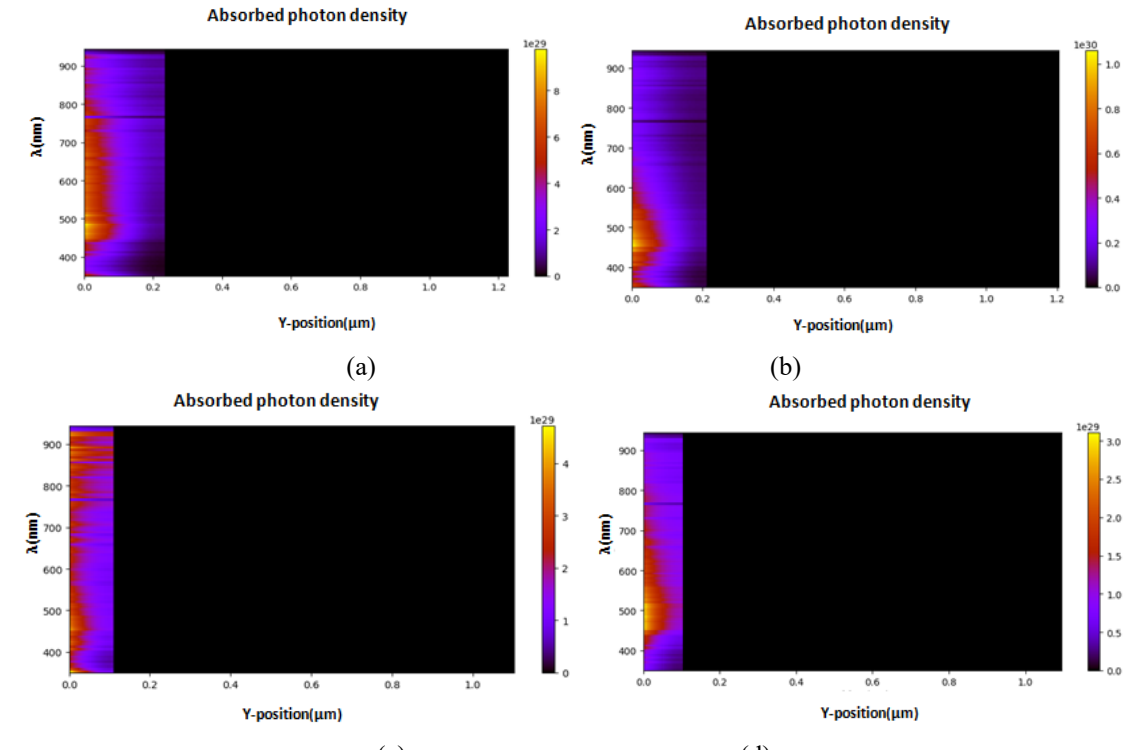

Figure 8 Absorbed photo density plots for samples developed at (a) 4000 (b) 5000 (c) 6000, and (d) 8000 RPM.

Table 1 Photon density, Absorbed photon density and Generation rate of films.

Absorbed photon density, Generation rate of films on the surface (Y=0) in presence of AM1.5G								
	11A4KMP		**11A5KMP**		**11A6KMP**		**11A8KMP**	
d_f(nm)	**234.1**		**210.8**		**108.3**		**100.1**	
	Y = 0	**Y = 234.1 (nm)**	**Y = 0**	**Y = 210.8 (nm)**	**Y = 0**	**Y = 108.3 (nm)**	**Y = 0**	**Y = 100.1 (nm)**
Photon density (m^{-3})	0.738	0.999	3.25E + 23	1.64E + 23	1.32E + 23	2.13E + 23	0.227	1
Absorbed photon density (m^{-3})	1	9.16 E − 07	1	1.16E − 06	4.33E + 29	1.17E + 25	1	3.40E − 06
Generation rate(m^{-3})	1.64E + 23	3.14 E + 17	2.82E + 23	3.29E + 17	3.43 E + 23	3.35E + 17	4.86E + 22	3.77E + 17

The film 11AKMP, which is used as the active layer in a graphical photovoltaic simulation, has dimensions of 2×2 cm^2 along x and z, and its thickness along -Y (-ve) direction. The optical and electrical properties of photovoltaic device layers are emulated by the GPVDM. With a light source of AM1.5g (1 sun = 100 mW/cm^2), the active layers of film 11AKMP were mimicked by varying the film thickness. The computed optical profile of the light is fed into the electrical simulation by the optical models, as seen in Figure 9. At every point in the apparatus, the absorbed photons are supplied by the optical model. The optical transfer matrix containing drift and diffusion equations of electron and hole is used to mimic external light incident on the device. Equations (1 and 2) are used to consider the experimental refractive index (n) and absorption coefficient (α)(m^{-1}) of the film as a function of λ(nm).

The absorption coefficient α (in m^{-1}) can be calculated from the transmittance (T) using the Beer–Lambert law, where alphaα = absorption coefficient (m^{-1}), d = thickness of the film (in meters) and T = transmittance (fraction, not percentage)

$$\alpha = \frac{1}{d} \ln\left(\frac{1}{T}\right) \tag{1}$$

If you have **reflectance (R)** data, the refractive index n can be estimated using the following formula (assuming negligible absorption in this region and normal incidence):

$$n = \frac{1 + \sqrt{R}}{1 - \sqrt{R}} \tag{2}$$

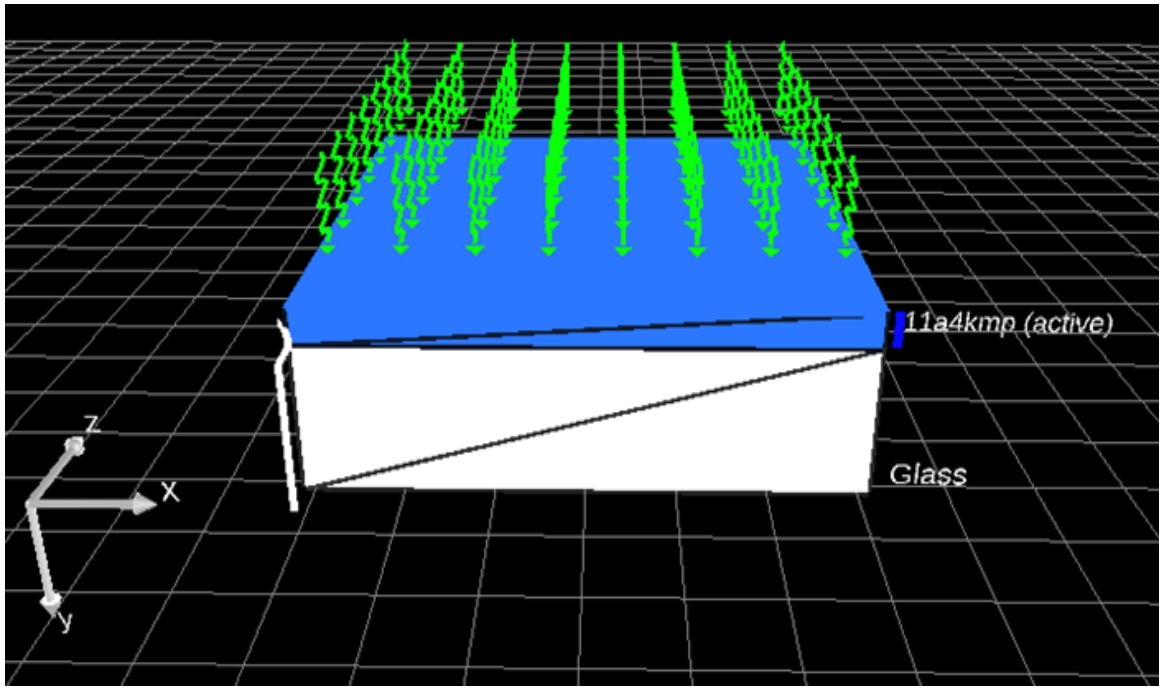

Figure 9 GPVDM layer design of film 11AKMP with size 2×2 cm^2.

Table 2 Microfilm solar cell parameters for low intensity condition, range of 349 - 950 nm.

Microfilm solar cell parameters for low intensity condition, range of 349 - 950 nm								
	11A4KMP		**11A5KMP**		**11A6KMP**		**11A8KMP**	
d_n(nm) **Film thickness**	**234.1** **2.7µm**		**210.8** **2.7µm**		**108.3** **2.7µm**		**100.1** **2.7µm**	
Sun Intensity	**5**	**20**	**5**	**20**	**5**	**20**	**5**	**20**
η_p(%)	0.1077	0.0108	0.0313	0.0104	0.0240	.1253	0.0294	0.0125
J_{sc}(A/m^2)	−5.7207	−8.5677	−6.2809	−8.4474	−6.3674	−5.5148	−5.0900	−7.7458
P_{max}(mW/m^2)	1.0779	2.1786	1.5670	2.0978	1.2015	1.253769	1.4735	1.8845
$V_{at\ max.power}$(10^{-1}V)	1.9945	2.8924	2.6941	2.5919	1.9939	2.9958	2.8949	2.8934
F.F(a.u)	1.2147	0.7949	0.8914	0.7797	0.9181	0.9823	1.3723	0.8084
V_{oc}(V)	0.1551	0.3198	0.2798	0.318475	0.2055	0.000	0.2109	0.3009

Table 2 shows microfilm solar cell parameters obtained for low intensity condition. The data highlights the performance of microfilm solar cells under low-intensity illumination (5% and 20%) across different configurations (11A4KMP to 11A8KMP). Sample 11A4KMP exhibits the highest efficiency (0.108%) at 5% intensity, while 11A6KMP shows an anomalously high value at 20% (0.125%) despite an Open circuit voltage (V_{oc}) of 0 V, indicating a possible measurement or calculation error. Generally, power output (Pmax) increases with light intensity, as expected, with the highest value (2.18 W/m²) observed in 11A4KMP at 20%. The short circuit current (J_{sc}) also increases with intensity, peaking in 11A4KMP and 11A5KMP. V_{oc} values range from 0.15 V to 0.32 V, with better voltage performance at higher light levels. The fill factor (FF) remains mostly below 1.4, though an outlier (∞) appears in 11A6KMP at 20%. Overall, 11A4KMP performs best in terms of balanced efficiency, voltage, and current, making it a strong candidate for low-light photovoltaic applications.

Conclusions

Higher transmittance was observed in the samples developed at higher spinning speeds which can be explained by the increase in transmittance. with reduction in thickness of the films. The electrical conductivity of the samples was measured and it was noted that the maximum conductivity of the films is of the order of 3×10^{-8} S/cm obtained in the case of ZTO+ MgF_2+PEDOT:PSS on glass substrate (sample-4) developed at 4000 RPM. Comparing both the optical and electrical characteristics, the sample-4 (ZTO + MgF_2 + PEDOT:PSS on glass substrate) has been selected for statistical analysis using GPVDM and is suggested for use in solar cells as a transparent electrode. SEM analysis for the chosen samples reavealed even distribution of particles. It was also evident that the film was coated perfectly forming a network. The thickness of the films formed at different spinning speeds was measured using ellipsometry, which showed that the thickness decreased as the spinning speed rose. The minimum thickness of the film was found to be 101.6 nm in the case of the samples developed at 8000 rpm. Finally, the I-V Characteristics of solar cell has been measured by using simulating software GPVDM. With increased rotation frequency of the film, the thickness decreased & the absorbed photon density was found to be increased. A lower absorbance at higher values of λ (nm) and vice versa was also observed. The refractive index has been decreased as the sample thickness has decreased and the optical conductivity has been found to be increased at higher wavelengths for samples developed at higher spinning speeds. As the thickness decreased, it was discovered that the conductivity rose, and all of the simulated outcomes and the experimental data agreed quite well. The efficiency also increased as the RPM increases and all the results are in consistence with previous works. Green synthesized ZTO nano material coated with Mgf_2 and PEDOT:PSS as thin films have the efficiency of 20.80% and open circuit voltage (V_{oc}) = 0.43. Based on the acquired results, it was determined that thin films covered with green synthesized ZTO nano material can serve as a viable substitute for the traditional transparent electrodes found in solar cells.

Acknowledgements

Authors are thankful to the in-organic chemistry lab for providing synthesis facilities, Nano technology laboratories of Department of Nano technology for providing UV-Visible characterization and Department of Instrument technology for providing electrical impedance spectroscopy for electrical characterization Andhra university, AP, India.

Declaration of Generative AI in Scientific Writing

The authors acknowledge the use of generative AI tools (e.g., QuillBot and ChatGPT by OpenAI) in the preparation of this manuscript, specifically for language editing and grammar correction. No content generation or data interpretation was performed by AI. The authors take full responsibility for the content and conclusions of this work.

CRediT Author Statement

Dr. Bhaskara Lakshmi and K. Saujanya conceived the study, led the experimental design, and wrote the first draft of the manuscript. Dr. A. Suneel Kumar contributed to the experimental design, conducted the statistical analysis, and provided critical feedback on the manuscript. Ravi Kota, Jayarangarao Prathipati, and Narasimhulu Tamminana assisted with data collection and performed the literature review. All authors contributed to the interpretation of the results and approved the final manuscript

References

[1] TA Gessert, J Burst, X Li, M Scott and TJ Coutts. Advantages of transparent conducting oxide thin films with controlled permittivity for thin film photovoltaic solar cells. *Thin Solid Films* 2011; **519(21)**, 7146-7148.

[2] FU Hamelmann. Transparent conductive oxides in thin film photovoltaics. *Journal of Physics: Conference Series* 2014; **559(1)**, 012016.

[3] J Liu, F Luo, A Wei, Z Liu and Y Zhao. In-situ growth of Cu_2ZnSnS_4 nanospheres thin film on transparent conducting glass and its application in dye-sensitized solar cells. Materials Letters 2015; **141**, 228-230.

[4] P Karthick, D Vijayanarayanan, M Sridharan, RTA Kumar, C Sanjeeviraja and K Jeyadheepan. Optimization of substrate temperature and

characterization of tin oxide based transparent conducting thin films for application in dye-sensitized solar cells. *Thin Solid Films* 2017; **631**, 1-11.

[5] BG Nair, H Rahman, V Sharma, GS Okram, U Deshpande, V Ganesan and RR Philip. Al doping for bipolarity induction in transparent conducting $CuInO_2$ and its application in diode fabrication. *Materials Science and Engineering: B* 2020; **255**, 114520.

[6] X Cao, S Sun, B Lu , Y Liu, R Ma, H Cao, H Ma and H Huang. Spectral photoluminescence properties of YAG:Ce,R (R: Gd^{3+}, Pr^{3+}, Gd^{3+} and Pr^{3+}) transparent fluorescent thin film prepared by pulse laser deposition. *Journal of Luminescence* 2020; **223**, 117222.

[7] A Karabulut, A Dere, AG Al-Sehemi, AA Al-Ghamdi and F Yakuphanoglu. Zinc oxide based 3-components semiconductor oxide photodiodes by dynamic spin coating method. *Materials Science in Semiconductor Processing* 2021; **134**, 106034.

[8] F Yakuphanoglu, B Gunduz, AA Al-Ghamdi, WA Farooq and F El-Tantawy. Transparent ultraviolet photodiodes based conductive gallium-indium-oxide films/p-type silicon for solar panel tracking systems. *Sensors and Actuators A: Physical* 2015; **234**, 212-222.

[9] MM Makhlouf. Preparation and optical characterization of β-MnO_2 nano thin films for application in heterojunction photodiodes. *Sensors and Actuators A: Physical* 2018; **279**, 145-156.

[10] BA Gozeh, A Karabulut, CB Ismael, SI Saleh and F Yakuphanoglu. Zn-doped CdO effects on the optical, electrical and photoresponse properties of heterojunctions-based photodiodes. *Journal of Alloys and Compounds* 2021; **872**, 159624.

[11] RR Kumar, Raghvendra, SK Pandey and SK Pandey. Experimental investigation and comparative analysis of electron beam evaporated ZnO/$Mg_xZn_{1-x}O$/$Cd_xZn_{1-x}O$ thin films for photodiode applications. *Superlattices and Microstructures* 2021; **150**, 106787.

[12] JW Han, B Jung, DW Kim, KT Lim, SY Jeong, and YH Kim. Transparent conductive hybrid thin-films based on copper-mesh/conductive polymer for ITO-free organic light-emitting diodes. *Organic Electronics* 2019; **73**, 13-17.

[13] A El-Shaer, W Ismail and M Abdelfatah. Towards low cost fabrication of inorganic white light emitting diode based on electrodeposited Cu_2O thin film/TiO_2 nanorods heterojunction. *Materials Research Bulletin* 2019; **116**, 111-116.

[14] N Saxena, P Manzhi, RJ Choudhary, S Upadhyay, S Ojha, GR Umapathy, V Chawla, OP Sicha and R Krishna. Performance optimization of transparent and conductive $Zn_{1-x}Al_xO$ thin films for opto-electronic devices: An experimental & first-principles investigation. *Vacuum* 2020; **177**, 109369.

[15] K Ueda, SH Kweon, H Hida, Y Mukouyama and I Kanno. Transparent piezoelectric thin-film devices: $Pb(Zr,Ti)O_3$ thin films on glass substrates. *Sensors and Actuators A: Physical* 2021; **327**, 112786.

[16] R Fan, R Peng, X Huang and M Wang. Making structured metals transparent for ultrabroadband electromagnetic waves and acoustic waves. *Annals of Physics* 2015; **358**, 5-19.

[17] M Ekmekcioglu, N Erdogan, AT Astarlioglu, S Yigen, G Aygun, L Ozyuzer and M Ozdemir. High transparent, low surface resistance ZTO/Ag/ZTO multilayer thin film electrodes on glass and polymer substrates. *Vacuum* 2021; **187**, 110100.

[18] MA Islam, KS Rahman, H Misran, N Asim, MS Hossain, M Akhtaruzzaman and N Amin. High mobility and transparent ZTO ETM prepared by RF reactive co-sputtering for perovskite solar cell application. *Results in Physics* 2019; **14**, 102518.

[19] I Arora, P Kumar, TS Sathiaraj and R Thangaraj. Structure, optical and electrical properties of sol-gel derived $Zn_{1.5+x}Sn_{1.5-x}O_4$ nanostructured films for optoelectronic applications. *Thin Solid Films* 2020; **698**, 137871.

[20] Q Zhang, G Xia, L Li, W Xia, H Gong and S Wang. High-performance zinc-tin-oxide thin film transistors based on environment-friendly solution process. *Current Applied Physics* 2019; **19(2)**, 174-181.

[21] S Lee, YH Joo and CI Kim. Influences of film thickness and annealing temperature on properties of sol-gel derived ZnO–SnO_2 nanocomposite thin film. *Applied Surface Science* 2014; **320**, 494-501.

[22] MF Zainal and Y Mohd. Characterization of PEDOT films for electrochromic applications.

Polymer-Plastics Technology and Engineering 2015; **57(3)**, 276-281.

[23] NC Das and PE Sokol. Hybrid photovoltaic devices from regioregular polythiophene and ZnO nanoparticles composites. *Renewable Energy* 2010; **35(12)**, 2683-2688.

[24] D Vanossi, L Cigarini, A Giaccherini, ED Como and C Fontanesi. An integrated experimental/theoretical study of structurally related poly-thiophenes used in photovoltaic systems. *Molecules* 2016; **21(1)**, 110.

[25] AK Mittal, Y Chisti and UC Banerjee. Synthesis of metallic nanoparticles using plant extracts. *Biotechnology Advances* 2013; **31(2)**, 346-356.

[26] S Ng, TJ Patey, R Buchel, F Krumeich, J Wang, HK Liu, SE Pratsinis and P Novak. Flame spray-pyrolyzed vanadium oxide nanoparticles for lithium battery cathodes. *Physical Chemistry Chemical Physics* 2009; **11(19)**, 3748-3755.

[27] D Manikprabhu and L Kattimani. Antibacterial activity of silver nanoparticles against methicillin-resistant Staphylococcus aureus synthesized using model Streptomyces sp. pigment by photo-irradiation method. *Journal of Pharmacy Research* 2013; **6(2)**, 255-260.

[28] RW Jones. *Fundamental principles of sol-gel technology*. Elsevier Science, Amsterdam, Netherlands, 1989.

[29] T Zhou, T Zhang, R Zhang, J Deng, Z Lou, G Lu and L Wang. Highly sensitive sensing platform based on $ZnSnO_3$ hollow cubes for detection of ethanol. *Applied Surface Science* 2017; **400**, 262-268.

[30] J Xu, X Jia, X Lou and J Shen. One-step hydrothermal synthesis and gas sensing property of $ZnSnO_3$ microparticles. *Solid-State Electronics* 2006; **50(3)**, 504-507.

[31] SK Sharma, DS Verma, LU Khan, S Kumar and S Khan. *Handbook of materials characterization.* Springer Nature, Cham, Switzerland, 2017.

[32] N Mayedwa, N Mongwaketsi, S Khamlich, K Kaviyarasu, N Matinise and M Maaza. Green synthesis of zinc tin oxide ($ZnSnO_3$) nanoparticles using Aspalathus linearis natural extracts: Structural, morphological, optical and electrochemistry study. *Applied Surface Science* 2018; **446**, 250-257.

[33] N Soin, P Zhao, K Prashanthi, J Chen, P Ding, E Zhou, T Shah, SC Ray, C Tsonos, T Thundat, E Siores and J Luo. High performance triboelectric nanogenerators based on phase-inversion piezoelectric membranes of poly(vinylidene fluoride)-zinc stannate (PVDF–$ZnSnO_3$) and polyamide-6 (PA6). *Nano Energy* 2016; **30**, 470-480.

[34] Y Chen, L Yu, Q Li, Y Wu, Q Li and T Wang. An evolution from 3D face-centered-cubic $ZnSnO_3$ nanocubes to 2D orthorhombic $ZnSnO_3$ nanosheets with excellent gas sensing performance. *Nanotechnology* 2012; **23(41)**, 415501.

[35] S Medda, A Hajra, U Dey, P Bose and NK Mondal. Biosynthesis of silver nanoparticles from Aloe vera leaf extract and antifungal activity against Rhizopus sp. and Aspergillus sp. *Applied Nanoscience* 2015; **5(7)**, 875-880.

[36] SA Khan, SB Khan, LU Khan, A Farooq, K Akhtar and AM Asiri. *Fourier transform infrared spectroscopy: fundamentals and application in functional groups and nanomaterials characterization*. Springer Nature, Cham, Switzerland, 2018.

[37] YV Bhaskaralakshmi, P Swapna, BK Babu and YS Rao. Green-synthesis, characterization and the biological evolution of ZnSnO3. *Asian Journal of Chemistry* 2022; **34(8)**, 2086-2090.

[38] V Panwar and G Anoop. Flexible piezoresistive strain sensor based on optimized elastomer-electronic polymer blend. *Measurement* 2021; **168**, 108406.

[39] S Long, K Yoon, L Dong-Ju and K Tae-Dong. Synthesis and characterization of PEDOT:PSS-PAs with good electrical conductivity for supercapacitor. *Chemical Science International Journal* 2023; **32(5)**, 13-25.

[40] R Kawamura and T Michinobu. PEDOT:PSS versus polyaniline: A comparative study of conducting polymers for organic electrochemical transistors. *Polymers* 2023; **15(24)**, 4657.